

THE CRYOGENIC REFRACTIVE INDICES OF S-FTM16, A UNIQUE OPTICAL GLASS FOR NEAR-INFRARED INSTRUMENTS

WARREN R. BROWN

Harvard-Smithsonian Center for Astrophysics, 60 Garden St, Cambridge, MA 02138

HARLAND W. EPPS

University of California Observatories/Lick Observatory, Santa Cruz, CA 95064

AND

DANIEL G. FABRICANT

Smithsonian Astrophysical Observatory, 60 Garden St, Cambridge, MA 02138

Accepted for publication in PASP, Sept 2004 issue

ABSTRACT

The Ohara glass S-FTM16 is of considerable interest for near-infrared optical designs because it transmits well through the K band and because negative S-FTM16 elements can be used to accurately achromatize positive calcium fluoride elements in refractive collimators and cameras. Glass manufacturers have sophisticated equipment to measure the refractive index at room temperature, but cannot typically measure the refractive index at cryogenic temperatures. Near-infrared optics, however, are operated at cryogenic temperatures to reduce thermal background. Thus we need to know the temperature dependence of S-FTM16's refractive index. We report here our measurements of the thermal dependence of S-FTM16's refractive index between room temperature and ~ 77 K. Within our measurement errors we find no evidence for a wavelength dependence or a nonlinear temperature term so our series of measurements can be reduced to a single number. We find that $\Delta n_{abs}/\Delta T = -2.4 \times 10^{-6} \text{ K}^{-1}$ between 298 K and ~ 77 K and in the wavelength range 0.6 μm to 2.6 μm . We estimate that the systematic error (which dominates the measurement error) in our measurement is 10%, sufficiently low for most purposes. We also find the integrated linear thermal expansion of S-FTM16 between 298 K and 77 K is $-0.00167 \text{ m m}^{-1}$.

Subject headings: instrumentation: infrared

1. INTRODUCTION

Optical designs of near-infrared (1.0 - 2.4 μm) instruments are strongly constrained by a limited selection of near-infrared optical materials. Low-index materials such as CaF₂, BaF₂, LiF, NaCl, and infrared grade fused quartz are commonly used for windows and simple achromatic doublets. However, these low-index materials have a restricted range of dispersive power that prevents good chromatic correction in complex, high-performance optical designs. In addition, NaCl, LiF, and BaF₂ are hygroscopic and prone to damage. Zinc Selenide (ZnSe) is another material suitable for near-infrared lenses, but its high index and large dispersive power limits its usefulness. In addition, the high index of ZnSe makes it difficult to design broadband anti-reflection coatings.

The internal transmission of most optical glasses with *intermediate* indices and dispersive powers is typically poor at near-infrared wavelengths, but the internal transmission of the glass S-FTM16 is a fortunate exception. Figure 1 shows that a 10-mm thick piece of S-FTM16 has an internal transmission of 98.7% at 2.0 μm and 95.3% at 2.4 μm . The dispersive power of S-FTM16 is $(dn/d\lambda)/(n-1) = -0.036155$ at 1.0 μm and $= -0.026242$ at 2.0 μm . To compare this with other infrared materials, we refer the reader to Table 1 of Epps & Elston (2002), which sorts twenty four infrared materials by dispersive power. The intermediate dispersive power of S-FTM16 is quite similar to the Schott glass TIFN5 and somewhat similar to the older Schott glass IRG7. However, TIFN5

and IRG7 are no longer available as stock glasses.

The intermediate dispersive power of S-FTM16 is extremely valuable for high-performance, near-infrared optical designs. For example, S-FTM16 is a critical part of the optical designs of FLAMINGOS-2, a near-infrared multi-slit spectrograph and imager for Gemini South (Epps & Elston 2002), and MMIRS, an instrument based on FLAMINGOS-2 for the f/5 MMT and Magellan telescopes (McLeod et al. 2004). Near-infrared astronomical instruments like FLAMINGOS-2 and MMIRS operate at liquid nitrogen temperatures (77 K) in order to reduce thermal background. The FLAMINGOS-2 and MMIRS optical designs are sensitive to index uncertainties of a few parts in 10^{-5} . Thus we need to know the refractive index, n , of S-FTM16 at cryogenic temperatures near ~ 77 K and at near-infrared wavelengths to be sure that the optics of FLAMINGOS-2 and MMIRS will perform properly.

Two large S-FTM16 blanks were purchased from Ohara Corporation for the FLAMINGOS-2 spectrograph optics. We had a small prism made from one of the blanks, and we sent the prism to Ohara to obtain melt indices. On 29 August 2003, Ohara obtained index measurements relative to air at room temperature (25 °C) and at sea level (760 torr). Measurement accuracy was stated to be $< \pm 1 \times 10^{-5}$. Table 1 presents the 12 optical/near-infrared lines we obtained. We were unable, however, to obtain cryogenic index measurements commercially.

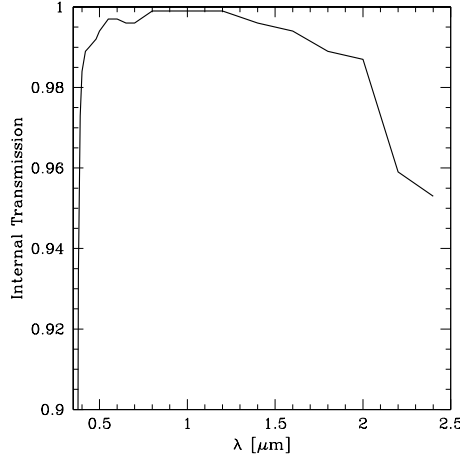


FIG. 1.— Internal transmission of a 10-mm thick piece of the intermediate-dispersion glass S-FTM16. (Values published by Ohara Corporation.)

Here, we report our measurements of $\Delta n/\Delta T$, the change in refractive index for S-FTM16 between room temperature and ~ 77 K. We will determine S-FTM16's cryogenic index by converting its melt indices in air to absolute indices in vacuum, and then adding our value of absolute $\Delta n/\Delta T$.

Physically, the temperature dependence of the refractive index depends on a material's density and its electrical properties (Fröhlich 1949). Materials expand and contract with temperature, thus density is temperature dependent. This is quantified by a material's coefficient of thermal expansion (CTE), which is wavelength independent. Electrically, a material can be neutral while its constituent atoms and ions have dipole moments that cause a macroscopic polarizability. The refractive index and dielectric constant depend on this macroscopic polarizability. The macroscopic polarizability is wavelength dependent. Because the ordering of microscopic dipole moments in a material depends on temperature, the macroscopic polarizability is also temperature dependent. Generally speaking, microscopic dipole moments will experience the most re-ordering near the melting point, and the least re-ordering near 0 K. This suggests we may not see a strong contribution from the macroscopic polarizability in our temperature regime. Interestingly, the refractive index changes due to density and polarizability are usually opposite in sign. Refractive index changes due to density tend to produce a negative dn/dT , and those due to polarizability tend to produce a positive dn/dT (Tropf et al. 1995). The balance of the two effects determines the final magnitude and sign of dn/dT .

The Ohara catalog contains thermo-optical measurements for S-FTM16, but for the limited temperature range -30 °C to $+70$ °C and for the limited wavelength range 0.435835 μm to 1.01398 μm. Table 2 summarizes the thermo-optical coefficients for S-FTM16 presented in the Ohara catalog, converted to an absolute dn/dT . Absolute dn/dT refers to a material with a vacuum/glass interface as opposed to a relative dn/dT which refers to an air/glass interface. Throughout this paper we discuss absolute dn/dT , or dn_{abs}/dT . It is apparent from Table 2 that dn_{abs}/dT of S-FTM16 varies with wavelength and

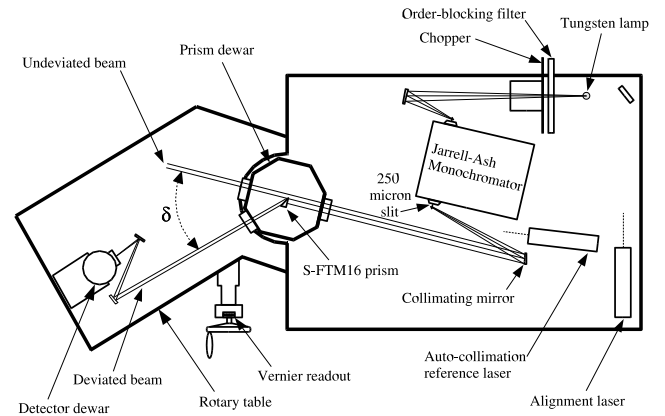


FIG. 2.— The layout of the Cryogenic Refractometer. The refractive index of the S-FTM16 prism at a given temperature and wavelength is found by measuring the angle δ between the deviated and undeviated beams. Figure based on a drawing by J. Palmer.

temperature. We note that the dependence of dn_{abs}/dT with wavelength and temperature decreases as the temperature drops and the wavelength increases, trends that are favorable for our application.

The paper is organized as follows. We begin in §2 by describing the experimental apparatus we used to measure S-FTM16's cryogenic refractive indices. We discuss the experimental data and errors in §3. We then present our measurements of S-FTM16's refractive index, thermo-optical coefficients, and cryogenic CTE in §4. We conclude in §5.

2. THE CRYOGENIC REFRACTOMETER

We used the Cryogenic Refractometer at the University of Arizona Optical Sciences Center to measure the change of the S-FTM16 refractive index between room and cryogenic temperatures. The Cryogenic Refractometer is an instrument built by J. Palmer and collaborators (Wolfe et al. 1980) that uses the modified minimum deviation method of Platt et al. (1975) to measure indices of refraction (see Figure 2). The advantage of the modified minimum deviation method is that it allows a prism to be mounted in a fixed cryogenic dewar. The disadvantage of the modified minimum deviation method is that it provides a less precise refractive index measurement compared to the more traditional minimum deviation and Littrow methods (because the collimated beam of light makes only a single pass through our prism). Optical glass manufacturers, using traditional methods, can provide index measurements with precisions as good as $\pm 1 \times 10^{-6}$ at room temperature. By comparison, our measurements have precisions of $\pm 3.5 \times 10^{-5}$ at cryogenic temperatures.

The layout of the Cryogenic Refractometer is shown in Figure 2. The refractometer measures the deviation angle, δ , of a collimated beam of light of wavelength λ that passes through a prism at temperature T . The prism's refractive index $n(\lambda, T)$ is found from

$$n(\lambda, T) = \frac{\sin(\alpha + \delta(\lambda, T))}{\sin \alpha} \quad (1)$$

where α is the apex angle of the prism and δ is the angle between the undeviated and deviated beams of light.

The test prism was mounted in a copper fixture inside the dewar. Temperatures between 60 K and 77 K were obtained by pumping on the LN₂ reservoir; temperatures between 77 K and 100 K were obtained with a heater adjacent to the prism. Temperatures were measured with two silicon diodes. One diode was located between the prism and the heater and the other was located on the copper fixture below the prism.

The refractometer uses a LN₂-cooled HgCdTe detector for 1.1 - 2.6 μm measurements and a room-temperature Si detector for 0.5 - 1.2 μm measurements. We measured the angle δ by rotating the detector on a precision rotary turntable (Société Genevoise PI-4) to locate the undeviated and deviated beams. The collimated beam was large enough to pass both through the prism (deviated) and around the prism (undeviated). We used a chopper and lock-in amplifier to improve the signal-to-noise of the beams.

We used a tungsten ribbon-filament lamp as the light source for all of our measurements. A 300 line mm^{-1} grating inside a Jarrell Ash Model 27 monochromator selected the desired wavelength. We used the 300 line mm^{-1} grating in first, second, and third orders to cover our full wavelength range. A 250 μm exit slit provided a spectral bandwidth ranging from 3 to 1 nm FWHM, depending on the grating order.

3. DATA AND ERRORS

3.1. Measurements

We measured the refractive index as follows. First, we allowed the prism temperature to stabilize. We then auto-collimated the prism to the collimated beam of light. We selected the desired wavelength with the Jarrell Ash monochrometer, using an order blocking filter as necessary. Finally, we rotated the arm holding the detector and located the undeviated and deviated beams. We repeated the last two steps until all wavelengths at a given temperature were measured.

The spatial profile of the collimated beam at the detector was the convolution of two narrow rectangle slits and so appeared approximately Gaussian in shape. To locate the peak of the profile, we obtained 5 to 10 observations around the centers of the undeviated and deviated beams. Each observation required manually rotating the turntable and reading the turntable's position with a vernier scale. We solved for the final deviation angle δ by fitting Gaussians to the undeviated and deviated profiles, and then calculating the angular difference between the centers of the beams.

3.2. Wavelengths and Temperatures

We measured the refractive index of S-FTM16 at 17 wavelengths between 0.546 μm and 2.600 μm and at 5 temperatures (62 K, 78 K \times 2, 87 K, 97 K, and 296 K). A second set of measurements at 296 K was obtained in air with the dewar windows removed. Table 3 summarizes the measured wavelengths: column 1 lists those wavelengths measured with the Si detector and column 2 lists those wavelengths measured with the HgCdTe detector.

We had planned to obtain additional measurements at temperatures between 100 K and room temperature, but the refractometer was unable to operate at these temperatures. We measured the undeviated and deviated beams

two to four times at each wavelength and temperature, yielding a raw data set of 3,246 individual observations and a reduced data set of 120 refractive indices. The measurements were obtained over five days in November 2003.

3.3. Errors

Our measurements contain both statistical and systematic errors. The systematic errors are much larger than the statistical errors, but the systematic errors are mostly removable. For example, we measure the wedge of the dewar windows by comparing room temperature measurements with and without the dewar windows in place. Similarly, we measure the focus offset between the Si and HgCdTe detectors by observing $\lambda = 1.129$ and $\lambda = 1.200 \mu\text{m}$ with both detectors. However, when we compare the Ohara melt indices with our room temperature measurements (see Figure 3), we find a residual systematic offset at the $\pm 10 \times 10^{-5}$ level that varies with wavelength. This systematic offset is likely due to mechanical error in the turntable. The Société Instruments Physique PI-4 is specified to have 5" accuracy, but the turntable we used was relatively old and the experimenter (W. Brown) noticed that the rotary handle had variable resistance in different areas. This suggests that the rotary mechanism has lost its original accuracy. We can fit and remove the systematic table error, but in doing so we would introduce additional uncertainty in the final index measurement.

We can avoid systematic errors altogether by focusing on the $\Delta n/\Delta T$ measurement of S-FTM16. The window wedge, detector offset, and rotary table error are independent of temperature, and so in principle cancel out when calculating $\Delta n/\Delta T$. The error in individual $\Delta n/\Delta T$ values is thus dominated by the statistical error in the index measurements.

Most of the sources of statistical error in the index measurements are angular uncertainties in the experimental apparatus that transform to uncertainties in the index n via Eqn. 1. Table 4 summarizes these errors.

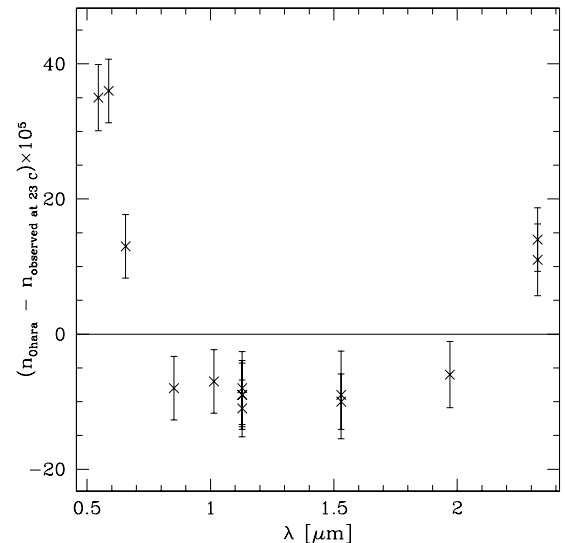


FIG. 3.— Difference between the Ohara melt values and our room temperature index measurements. The shape of the offset is the same at all temperatures, and is likely due to mechanical error in the turntable.

3.3.1. Deviation Angle

We estimate the error in the deviation angle measurement from the residuals of the Gaussian profile fits. The residuals of the Gaussian profile fits are typically $\pm 4.1''$ for the Si detector and $\pm 5.1''$ for the HgCdTe detector. Summing the undeviated and deviated beam uncertainties in quadrature, the uncertainty in the deviation angle contributes errors of $\pm 2.1 \times 10^{-5}$ and $\pm 2.8 \times 10^{-5}$ to n for the Si and HgCdTe detectors, respectively.

3.3.2. Apex Angle

We measured the apex angle α of the S-FTM16 prism on a Wild 79 spectrometer. The average of ten measurements was $\alpha = 34^\circ 59' 38'' \pm 3''$. This is statistically identical to Ohara Corporation's measurement of the apex angle, $\alpha_{\text{Ohara}} = 34^\circ 59' 39'' \pm 3''$. The $\pm 3''$ uncertainty in the apex angle contributes an error of $\pm 2.2 \times 10^{-5}$ to n , and has a small wavelength dependence.

3.3.3. Autocollimation

The deviation angle measurement assumes that the prism is aligned with the undeviated collimated beam of light. The autocollimation of the prism is set by aligning the retro-reflected beam from the prism face onto the exit slit of the Jarrell Ash monochromator. The retro-reflected beam can be set with an uncertainty of $\pm 0.5''$. We maintain the autocollimation by shining a He-Ne laser onto the prism face and making sure the reflected spot on the wall (~ 8 m away) does not move. If the prism shifts (i.e. due to changes in temperature) we tip/tilt the dewar to compensate. The laser spot center can be maintained to $\pm 0.75''$. Summing these uncertainties in quadrature, the autocollimation of the prism contributes an error of $\pm 0.3 \times 10^{-5}$ to n .

3.3.4. Wavelength

We calibrated the wavelength readings on the Jarrell Ash spectrometer with higher orders of a He-Ne alignment laser. A linear fit with wavelength leaves excessive residuals, and so our final calibration uses a cubic fit. The residuals of the fit are ± 0.20 nm. In addition, the dial on the spectrometer was read with a precision of ± 0.28 nm. Summing these uncertainties in quadrature, the total error in the wavelengths is ± 0.34 nm. Propagating this through the Schott equation shows that the wavelength uncertainty contributes an error of $\pm 0.5 \times 10^{-5}$ to n .

3.3.5. Temperature

We average the temperature readings of the diodes above and below the prism to obtain the prism temperature. Because the observed temperature gradient across the prism is always less than 1°C at equilibrium, we conservatively estimate the uncertainty in the prism temperature to be $\pm 0.5^\circ\text{C}$. Propagating this through a dn/dT relation shows that the temperature uncertainty contributes an error of $\pm 0.2 \times 10^{-5}$ to n .

4. RESULTS AND DISCUSSION

4.1. Room Temperature n

The $\pm 1 \times 10^{-5}$ accuracy of the Ohara melt information is superior to our measurements, and so we report Ohara's melt values for S-FTM16's room temperature

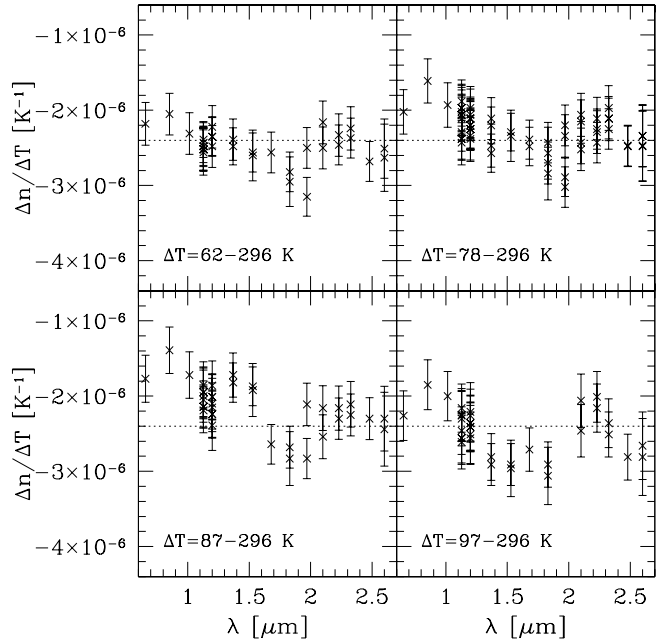


FIG. 4.— Values of $\Delta n/\Delta T$ calculated between our four cryogenic temperatures and room temperature. Dotted lines show the average value $\Delta n/\Delta T = -2.4 \times 10^{-6} \pm 0.3 \times 10^{-6} \text{ K}^{-1}$ for all temperature differences.

index relative to air (Table 1). We fit the Ohara melt values with the six coefficient Schott formula,

$$n^2 = A0 + A1\lambda^2 + A2\lambda^{-2} + A3\lambda^{-4} + A4\lambda^{-6} + A5\lambda^{-8}, \quad (2)$$

where λ is in μm . The best-fit Schott coefficients are presented in Table 5. The residuals of the best-fit Schott function are $\pm 0.55 \times 10^{-5}$ in n . It is important to obtain melt information because S-FTM16's refractive index will vary from melt to melt.

Because this paper is primarily concerned with absolute indices, Table 5 also presents the best-fit Schott coefficients for S-FTM16 in vacuum. We correct the Ohara indices from air to vacuum by multiplying the indices by the refractive index of air $n(\lambda)_{25,760}$. The refractive index of air at 25°C , 760 torr, and in the wavelength range 1 to $2.6 \mu\text{m}$ is $n(\lambda)_{25,760} \simeq 1.00026$ (Filippenko 1982), with a well-determined wavelength dependence at the 10^{-7} level. The air-to-vacuum transformation adds negligible error to the values of n .

4.2. Cryogenic n and dn/dT

We determine S-FTM16's absolute cryogenic refractive index by calculating the difference between our cryogenic and room temperature vacuum measurements. Calculating the difference in index minimizes the effects of systematic errors and any uncertainty in the calibration of our data. Our series of absolute index measurements thus reduces to a series of absolute $\Delta n/\Delta T$ values between ~ 77 K and room temperature. We look for wavelength-dependent terms in the $\Delta n/\Delta T$ values, but, because of the relatively coarse $\pm 3.5 \times 10^{-5}$ precision of our indices, we do not find wavelength- or temperature-dependent terms statistically significant. Our vacuum indices provide a direct measurement of absolute $\Delta n/\Delta T$.

Figure 4 plots the values of absolute $\Delta n/\Delta T$ between our four cryogenic temperatures and room temperature.

Measurements are plotted against wavelength. We have two data sets at room temperature that we use as comparison. The room temperature measurements in air have been corrected to vacuum. The grand average of all the values, shown by the dotted line in Figure 4, is $\Delta n_{abs}/\Delta T = -2.4 \times 10^{-6} \pm 0.3 \times 10^{-6} \text{ K}^{-1}$.

We see apparent wavelength-dependent structure in the $\Delta n/\Delta T$ measurements, but we determine that this wavelength-dependent structure is not significant with respect to a constant fit. Figure 5 plots all of our $\Delta n/\Delta T$ measurements together. Physically, we expect $\Delta n/\Delta T$ to have wavelength dependence, but we expect the wavelength dependence to be small at our temperatures and near-infrared wavelengths. When we test high order wavelength fits to the $\Delta n/\Delta T$ data set, we find that the reduced χ^2 and the RMS residuals do not significantly improve with respect to a constant $\Delta n/\Delta T$. For example, the linear fit in Figure 5 reduces the RMS residuals by a mere 6%. Furthermore, the linear fit deviates from a constant $\Delta n/\Delta T$ by $\pm 0.1 \times 10^{-6} \text{ K}^{-1}$ (a factor of three smaller than our uncertainty) within the wavelength range 1 μm to 2.6 μm . We plot values of $\Delta n/\Delta T$ averaged over temperature (lower panel, Figure 5) to further explore the possibility of wavelength-depen-

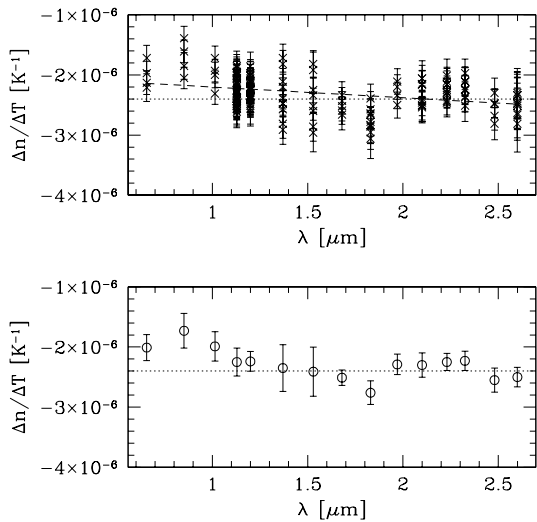


FIG. 5.— The upper panel shows all $\Delta n/\Delta T$ measurements plotted together; the dashed line is the linear best fit to the data and does not significantly improve the residuals. The lower panel shows the $\Delta n/\Delta T$ values averaged over temperature, with the error bars showing the RMS. The horizontal dotted lines show our final fit $\Delta n/\Delta T = -2.4 \times 10^{-6} \pm 0.3 \times 10^{-6} \text{ K}^{-1}$.

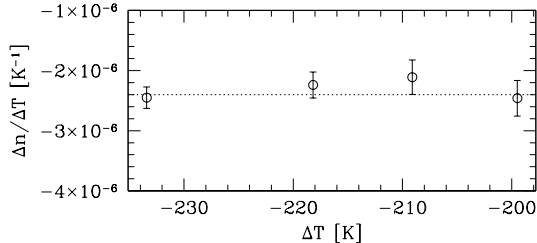


FIG. 6.— Values of $\Delta n/\Delta T$ averaged over wavelength. Error bars show the RMS of the $\Delta n/\Delta T$ values at that temperature. The dotted line shows our final fit $\Delta n/\Delta T = -2.4 \times 10^{-6} \pm 0.3 \times 10^{-6} \text{ K}^{-1}$.

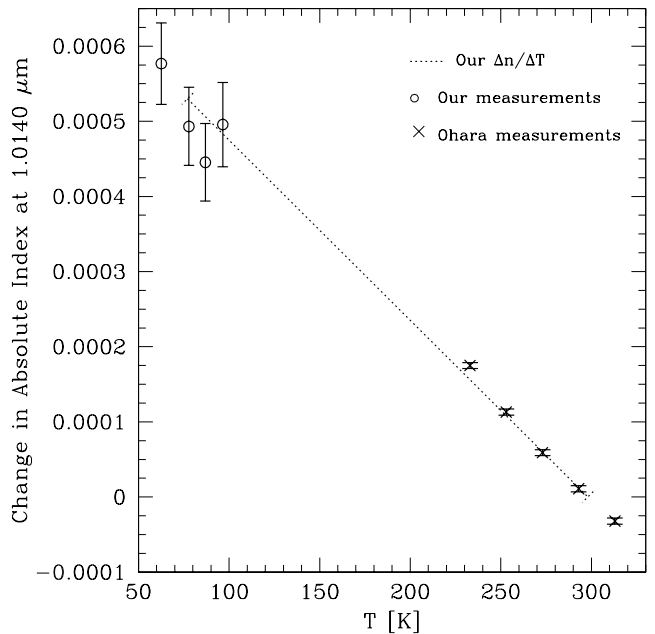


FIG. 7.— A comparison of our absolute $\Delta n/\Delta T$ value and Ohara absolute $\Delta n/\Delta T$ values integrated over appropriate ranges in temperature. The change in absolute index is normalized to 0 at 298 K. The dotted line shows our final fit $\Delta n_{abs}/\Delta T = -2.4 \times 10^{-6} \pm 0.3 \times 10^{-6} \text{ K}^{-1}$ between 298 K and 77 K, which nicely matches the Ohara $\Delta n/\Delta T$ values near room temperature.

dent structure. The error bars show the RMS of the $\Delta n/\Delta T$ values at that wavelength. Only one of the 15 points differs by 2σ from a constant $\Delta n/\Delta T$; eleven points agree to better than 1σ with a constant $\Delta n/\Delta T$. Thus the data appears well described by a constant $\Delta n/\Delta T$. Because the error on the mean is negligible, we conclude that the $\pm 0.3 \times 10^{-6} \text{ K}^{-1}$ uncertainty is dominated by residual systematic errors in the measurements.

We now investigate temperature dependence in the $\Delta n/\Delta T$ measurements. Figure 6 plots the $\Delta n/\Delta T$ values averaged over wavelength. Error bars show the RMS for the $\Delta n/\Delta T$ values at that temperature. Our cryogenic measurements span 62 K to 97 K, and we see no obvious trend in this range of temperatures. Thus $\Delta n/\Delta T$ is well described by a constant value in the temperature range 62 K to 97 K.

We compare with Ohara catalog dn/dT values as a check of our measurements. Note that we measure a single, integrated $\Delta n/\Delta T$ value between room temperature and liquid nitrogen temperatures while Ohara, on the other hand, measures dn/dT in small temperature and wavelength ranges. A comparison can be made only if we integrate the dn/dT values over temperature and compare the changes in index, Δn . Figure 7 shows the change in absolute index at 1.0140 μm , normalized to 0 at 298 K, for Ohara's integrated dn/dT values and our $\Delta n/\Delta T$ measurements (from Figure 6). The dotted line in Figure 7 shows our $\Delta n_{abs}/\Delta T = -2.4 \times 10^{-6} \pm 0.3 \times 10^{-6} \text{ K}^{-1}$ between 298 K and 77 K. Our $\Delta n/\Delta T$ nicely matches the Ohara $\Delta n/\Delta T$ values near room temperature.

The cryogenic index of S-FTM16 in vacuum is found by adding the Δn for the desired ΔT . Going from room

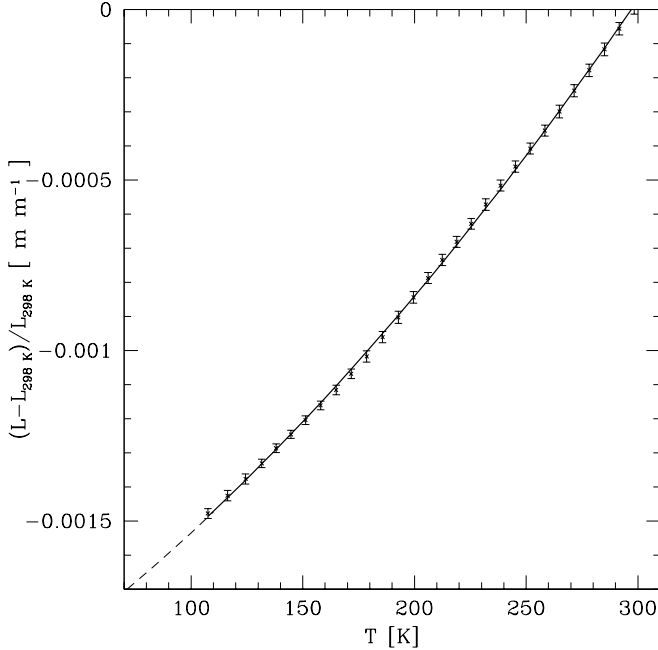


FIG. 8.— Integrated linear thermal expansion of S-FTM16 with respect to 298 K. The solid line shows the best-fit quadratic, and the dashed line shows the extrapolation of this fit to 70 K.

temperature 298 K to liquid nitrogen temperature 77 K, the absolute $\Delta n_{298 \rightarrow 77\text{K}} = +53 \times 10^{-5} \pm 7 \times 10^{-5}$ (see Figure 7).

Finally, we investigate the effect of the 10% uncertainty in $\Delta n/\Delta T$ on a high-performance optical design. The MMT Magellan InfraRed Spectrograph (MMIRS) optical design, for example, uses two S-FTM16 elements in the camera (McLeod et al. 2004). Changing S-FTM16 in MMIRS by $\Delta n = \pm 10 \times 10^{-5}$ results in a small 0.3% change in RMS spot size and a $\pm 25 \mu\text{m}$ re-focus. Thus our 10% determination of $\Delta n/\Delta T$ is more than adequate to maintain the high performance of the MMIRS optical design.

4.3. Cryogenic Coefficient of Thermal Expansion

We obtain cryogenic CTE measurements so that properly athermalized lens mounts can be designed for S-FTM16. On 13 April 2004 Harrop Industries, Inc, performed a thermal dilatometric analysis on a sample of S-FTM16 cut from the same block as our prism. The S-FTM16 sample was first cooled to 100 K (colder temperatures were not possible with the apparatus), and then the sample's length was measured with a dilatometer as it slowly warmed up. The result is a direct measurement of S-FTM16's integrated linear thermal expansion between 100 K and 298 K.

Figure 8 shows S-FTM16's integrated linear thermal expansion with respect to 298 K. There is a clear second-order term in the data, and the solid line shows the best-fit quadratic

$$(L - L_{298\text{K}})/L_{298\text{K}} = -2.05 \times 10^{-3} + 4.27 \times 10^{-6}T + 8.84 \times 10^{-9}T^2 \quad (3)$$

where L is the length at temperature T (in K), and $L_{298\text{K}}$ is the length at 298 K. The dashed line in Figure 8 shows the extrapolation of this fit to 70 K. The integrated linear

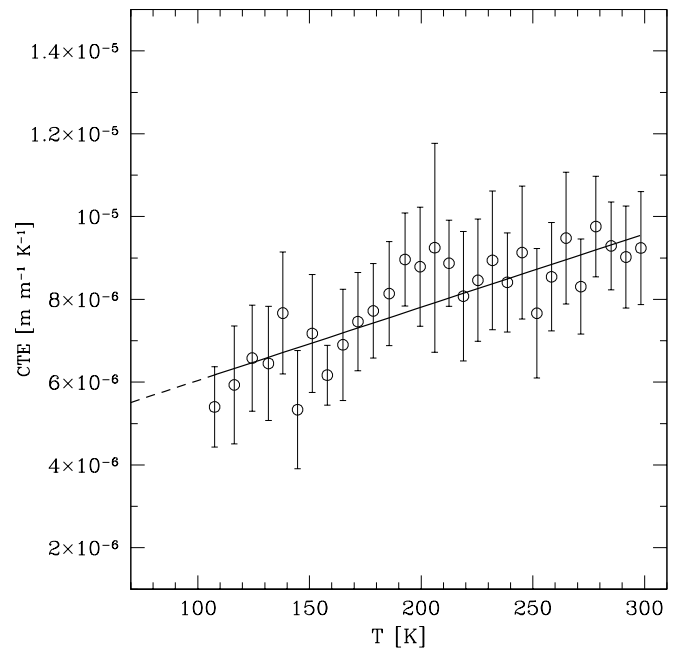


FIG. 9.— S-FTM16's linear coefficient of thermal expansion with temperature. The solid line shows the best-fit line, and the dashed line shows the extrapolation of this fit to 70 K.

thermal expansion of S-FTM16 between 298 K and 77 K is $-0.00167 \pm 0.00001 \text{ m m}^{-1}$.

Figure 9 shows S-FTM16's CTE with temperature. The CTE is simply the slope of the integrated linear thermal expansion line at a given temperature. The CTE values in Figure 9 are calculated by binning 16 dilatometer measurements together in approximately 9 K intervals; the error bars show the RMS of the measurements in a given bin. The solid line drawn through the CTE values in Figure 9 is given by

$$\text{CTE} = 4.27 \times 10^{-6} + 1.77 \times 10^{-8}T, \quad (4)$$

where CTE has units of $\text{m m}^{-1} \text{ K}^{-1}$ and T has units of K. The dashed line in Figure 9 shows the extrapolation of this fit to 70 K. We find that S-FTM16's CTE is a smoothly varying, positive quantity between 100 K and 298 K, consistent with our $\Delta n/\Delta T$. Ohara reports a CTE of $9 \times 10^{-6} \text{ m m}^{-1} \text{ K}^{-1}$ between 240 K and 340 K, which is in good agreement with our CTE measurements.

5. CONCLUSIONS

The glass S-FTM16 is an important addition to the list of optical materials for near-infrared instruments. The glass has $> 95\%$ internal transmission out to $2.4 \mu\text{m}$, and is currently the only intermediate dispersion material available to near-infrared optical designs. High-performance optical designs require accurate knowledge of material properties, especially at the cryogenic temperatures at which near-infrared instruments operate. Thus we have undertaken cryogenic refractive index measurements for S-FTM16.

Our measurements were made with the Cryogenic Refractometer at the University of Arizona. The experimental apparatus uses the modified minimum deviation method to measure refractive index. Individual measurements have $\pm 3.5 \times 10^{-5}$ precision in n . We use Ohara's

TABLE 1
OHARA S-FTM16 INDICES^a

| λ (μm) | n_{rel} | $\sigma_n \times 10^5$ |
|-----------------------------|-----------|------------------------|
| 0.435835 | 1.61528 | 1.0 |
| 0.486133 | 1.60529 | 1.0 |
| 0.546075 | 1.59737 | 1.0 |
| 0.587562 | 1.59338 | 1.0 |
| 0.63280 | 1.58997 | 1.0 |
| 0.656273 | 1.58847 | 1.0 |
| 0.85211 | 1.58028 | 1.0 |
| 1.01398 | 1.57636 | 1.0 |
| 1.12864 | 1.57423 | 1.0 |
| 1.52958 | 1.56830 | 1.0 |
| 1.97009 | 1.56215 | 1.0 |
| 2.32542 | 1.55674 | 1.0 |

^aAt standard air (T, P) = (25 °C, 760 torr).

TABLE 2
OHARA VALUES OF S-FTM16's ABSOLUTE dn/dT

| Temp (°C) | dn_{abs}/dT ($10^{-6}/\text{°C}$) | | | | | |
|-----------|---------------------------------------|------------------|------------------|------------------|------------------|------------------|
| | $\lambda 0.4358$ | $\lambda 0.4800$ | $\lambda 0.5461$ | $\lambda 0.5893$ | $\lambda 0.6328$ | $\lambda 1.0140$ |
| -30 | -0.8 | -1.5 | -2.2 | -2.4 | -2.6 | -3.1 |
| -10 | -0.3 | -1.1 | -1.7 | -1.8 | -2.1 | -2.7 |
| 10 | 0.2 | -0.6 | -1.3 | -1.5 | -1.8 | -2.4 |
| 30 | 0.7 | -0.2 | -0.9 | -1.2 | -1.5 | -2.1 |
| 50 | 1.0 | 0.2 | -0.6 | -0.9 | -1.2 | -1.8 |
| 70 | 1.4 | 0.5 | -0.4 | -0.7 | -1.0 | -1.6 |

high accuracy melt information to define S-FTM16's relative refractive index at room temperature. We convert the relative indices to absolute indices. We then use our vacuum measurements to calculate the change in S-FTM16's refractive index between room temperature and 77 K, independent of systematic errors.

We find $\Delta n_{abs}/\Delta T = -2.4 \times 10^{-6} \pm 0.3 \times 10^{-6} \text{ K}^{-1}$, valid in the wavelength range 0.6 μm to 2.6 μm and between room temperature and liquid nitrogen temperatures. This corresponds to an absolute $\Delta n_{298 \rightarrow 77\text{K}} = +53 \times 10^{-5} \pm 7 \times 10^{-5}$ between 298 K and 77 K. We find no statistical evidence for wavelength- or temperature-dependent terms to the uncertainty of our measurements. The 10% accuracy of our $\Delta n/\Delta T_{abs}$ determination is more than adequate to maintain the high-performance of the MMIRS optical design. The integrated linear ther-

mal expansion of S-FTM16 between 298 K and 77 K is $-0.00167 \pm 0.00001 \text{ m m}^{-1}$.

We are grateful to the late Richard J. Elston for his interest and support. Richard provided the S-FTM16 glass samples as part of the FLAMINGOS-2 project. We also thank Dr. Jim Palmer for allowing us to use the Cryogenic Refractometer, and for his assistance with set-up and measurements. Funding for this project was provided in part by W. Brown's Harvard-Smithsonian CfA Fellowship. The cryogenic CTE measurements were paid by the MMIRS project, supported by AURA through the National Science Foundation under AURA Cooperative Agreement AST 0132798, as amended.

REFERENCES

Epps, H. W. & Elston, R. J. 2002, in Proc. SPIE, Vol. 4841, Instrument Design and Performance for Optical/Infrared Ground-based Telescopes, ed. M. Iye & A. Moorwood, 1280–1294

Filippenko, A. V. 1982, PASP, 94, 715

Fröhlich, H. 1949, Theory of Dielectrics (London: Oxford University Press)

McLeod, B. A., Geary, J., Fabricant, D., Epps, H., Nystrom, G., Elston, R., & Martini, P. 2004, in Proc. SPIE, Vol. 5492, Ground-based Instrumentation for Astronomy, ed. A. Moorwood & M. Iye

Platt, B. C., Icenogle, H. W., Harvey, J. E., Korniski, R. J., & Wolfe, W. L. 1975, J. Opt. Soc. Am. A, 65, 1264

Tropf, W. J., Thomas, M. E., & Harris, T. J. 1995, in Handbook of Optics, ed. M. Bass, E. W. Van Stryland, D. R. Williams, & W. L. Wolfe, Vol. 2 (McGraw-Hill, Inc.), 33.28

Wolfe, W. L., Debell, A. G., & Palmer, J. M. 1980, in Proc. SPIE, Vol. 245, Cryogenically Cooled Sensor Technology, ed. R. J. Huppi, 164–172

TABLE 3
WAVELENGTHS
MEASURED

| $\lambda(\text{Si})$ μm | $\lambda(\text{HgCdTe})$ μm |
|---------------------------------------|---|
| 0.546 | 1.129 |
| 0.588 | 1.200 |
| 0.656 | 1.370 |
| 0.852 | 1.530 |
| 1.014 | 1.680 |
| 1.129 | 1.830 |
| 1.200 | 1.970 |
| | 2.100 |
| | 2.230 |
| | 2.325 |
| | 2.480 |
| | 2.600 |

TABLE 4
SUMMARY OF STATISTICAL ERRORS

| Error Source | Si $\sigma_n \times 10^5$ | HgCdTe $\sigma_n \times 10^5$ |
|-----------------------------|------------------------------|----------------------------------|
| Deviation angle measurement | 2.1 | 2.8 |
| Apex angle measurement | 2.2 | 2.1 |
| Autocollimation alignment | 0.3 | 0.3 |
| Wavelength setting | 0.5 | 0.5 |
| Temperature uncertainty | 0.2 | 0.2 |
| | == | == |
| TOTAL ERROR | 3.1 | 3.6 |

TABLE 5
S-FTM16 SCHOTT COEFFICIENTS

| Schott coef | $(T, P) = (+25^\circ\text{C}, 760 \text{ torr})$ | $(T, P) = (+25^\circ\text{C}, 0 \text{ torr})$ |
|-------------|--|--|
| A0 | 2.47395 | 2.47522 |
| A1 | -1.00689×10^{-2} | -1.00713×10^{-2} |
| A2 | 2.10265×10^{-2} | 2.11039×10^{-2} |
| A3 | 9.30325×10^{-4} | 8.93809×10^{-4} |
| A4 | -3.30921×10^{-5} | -2.44143×10^{-5} |
| A5 | 7.08359×10^{-6} | 6.41271×10^{-6} |